



CHORUS

This is the accepted manuscript made available via CHORUS. The article has been published as:

Picosecond Absorption Spectroscopy of Excited States in BaBrCl with and without Eu Dopant and Au Codopant

Peiyun Li, Sergii Gridin, K. Burak Ucer, Richard T. Williams, Mauro Del Ben, Andrew Canning, Federico Moretti, and Edith Bourret

Phys. Rev. Applied **12**, 014035 — Published 19 July 2019

DOI: [10.1103/PhysRevApplied.12.014035](https://doi.org/10.1103/PhysRevApplied.12.014035)

Picosecond absorption spectroscopy of excited states in BaBrCl with and without Eu dopant and Au codopant

Peiyun Li, Sergii Gridin, K. Burak Ucer, and Richard T. Williams*
Department of Physics, Wake Forest University, Winston Salem, NC 27106, USA

Mauro Del Ben, Andrew Canning, Federico Moretti, and Edith Bourret
Lawrence Berkeley National Laboratory, Berkeley, CA 94720, USA

(Dated: June 18, 2019)

We measure picosecond absorption spectroscopy on BaBrCl samples that are undoped, doped with europium to make activated scintillators, and codoped with gold (as AuBr₃ in the melt) to increase light yield. The time-resolved measurements provide insights on effects of interband excitation in BaBrCl including identification of self-trapped exciton (STE) absorption bands, the mechanism of energy transport from the host to the Eu activator, and effects of Au co-doping. First principles electronic structure calculations of STE relaxations in BaBrCl are presented. BaBrCl:Eu:Au is a beneficiary of two material modifications for improvement of performance that are intensely investigated recently – a mixed-halide solid solution that is further modified by aliovalent co-doping.

I. INTRODUCTION

Among scintillation materials for energy-resolving detection of ionizing radiation, two of the best performing ones that have reached commercialization are LaBr₃:Ce and SrI₂:Eu. LaBr₃:Ce with Sr codopant holds the current record for gamma energy resolution by a scintillator, $\Delta E/E=2.0\%$ at 662 keV [1]. SrI₂:Eu probably holds the current record for light yield among commercialized scintillators, measured in the range of 90,000 - 120,000 photons/MeV [2–4]. While these are respective paradigms of two important technical performance criteria, both scintillators are expensive, both are very hygroscopic, and SrI₂:Eu needs pulse shape analysis to overcome a problem with self-absorption of the Eu scintillation light [5]. Cost and ruggedness are important concerns in most applications, and strategically so for security screening where widespread deployment is crucial. On several grounds, there remain reasons to continue searching for high-performance scintillators that are cheaper, e.g. due to ease of crystal growth, and are less hygroscopic.

In the same chemical family with SrI₂:Eu but with even higher density and effective atomic number, BaI₂:Eu has been investigated as a scintillator. However, it exhibits a light yield of only about 38,000 photons/MeV [6–8]. It was found roughly concurrently that trading the pure iodide anions for a 50/50 halide mixture of Br and I in a barium mixed halide salt yields decidedly better performance [9, 10]. BaBrI:Eu scintillator crystals exhibit excellent light yield of 97,000 photons/MeV and energy resolution of 3.4% at 662 keV [10]. A number of barium mixed halides and mixed barium alkali iodides were also found to have good scintillation properties [11, 12]. This may be part of the empirical trend noted by Gektin et al that mixed ion crystals and solid solutions often ex-

hibit better scintillation performance in light yield and resolution than do the pure single-halide or single-cation versions [13]. Even with its excellent scintillation characteristics, BaBrI:Eu is still hygroscopic and relatively difficult to grow in large size, so the search for good scintillators within the barium mixed halide family continued, including demonstration of good performance and relative ease of crystal growth in BaBrCl:Eu [14]. The BaBr₂-BaCl₂ system forms a solid solution at all concentrations. Crack-free transparent crystals of BaBrCl can be grown and the best reported performance in 5% Eu-doped BaBrCl includes light yield of 55,000 ph/MeV and energy resolution of 3.55% at 662 keV in a small crystal [14].

Some members of the general barium mixed halide BaXY family, especially BaFBr:Eu are well known as storage phosphors for x-ray imaging [15–17]. The F center (halide vacancy trapping an electron) is found to play an essential role as a temporary electron trap, i.e. the storage step in the storage phosphor. The electron binding energy of the F center in different members of the BaXY family at room temperature controls whether the material functions as a storage phosphor or possibly as a scintillator [18]. BaBrCl:Eu is one of the scintillators in this family as noted above.

Our opening example of LaBr₃:Ce:Sr illustrates the remarkable success of aliovalent co-doping in improving the already excellent performance of LaBr₃:Ce. The success of LaBr₃:Ce:Sr helped promote widespread investigation of effects of co-doping on performance of other scintillators [19–24]. Co-doping turns out to be helpful in a number of scintillator materials, but particularly in halide scintillators the reasons are not always well understood and likely not always the same. The present study deals with a finding by Shalapska, et al that co-doping BaBrCl:Eu with trivalent Au (gold) produces a significant improvement of light yield. It was shown that 0.1 mole% AuBr₃ codoping in the melt tripled the scintillation light yield of 0.5% Eu-doped BaBrCl and made a

* williams@wfu.edu

TABLE I. Some properties of the BaBrCl samples studied in this work. Concentrations are given as mole% in the melt.

Crystal	Eu, mole%	Au, mole%	Thickness, mm
BaBrCl:undoped	0	0	2.05
BaBrCl:Au	0	0.05	3.55
BaBrCl:Eu	0.5	0	2.3
BaBrCl:Eu,Au	0.5	0.1	2.2

40% improvement in 5% Eu-doped crystals. At the same time, Au co-doping diminished the slow component of scintillation decay, so-called afterglow [25].

II. EXPERIMENT

A. Sample characteristics

The BaBrCl crystals were grown by the vertical Bridgman-Stockbarger method in vacuum sealed quartz ampoules using high purity (99.999%) BaBr₂, BaCl₂, EuBr₂, and AuBr₃ from Sigma-Aldrich. Raw material handling and crystal cutting and polishing was done in an Ar-filled glove box with H₂O and O₂ concentration below 0.1 ppm. Prior to growth, the raw materials were dried in vacuum at 120 C overnight and the ampoule was subsequently sealed under vacuum. The crystals were grown at 0.78 mm/h.

The obtained crystals are transparent, though the Au (co-) doped ones are characterized by the presence of a metallic gold layer on top of the boule (Fig. 1(a)), and the presence of molecular bromine is seen as an orange coloration of the ampoule (Fig. 1(b)) suggesting that AuBr₃ is not stable at these growth conditions and it undergoes dissociation. Br₂ that is volatile at room temperature fills all empty spaces of the ampoule and is clearly seen in the top part above the crystal. The color disappears quickly when the ampoule is opened, allowing the bromine gas to disperse in the dry-box. For the transient spectroscopy, the samples cut from the boules were polished and encapsulated in cells with fused quartz windows while in a nitrogen-filled glove box with O₂ < 0.07 ppm and H₂O < 0.28 ppm. A list of the samples and their properties is given in Table I.

Impurity and Au content in representative BaBrCl as-grown crystals without and with doping was measured by Glow Discharge Mass Spectrometry (GDMS). The main impurities detected are Na (few ppm wt.), I (170 ppm wt.), and Ca (few ppm wt.). Data obtained on O, C, S are not reliable due to possible environmental contamination during sample preparation. GDMS data on a melt-quenched BaBrCl:Eu sample co-doped in the melt with 0.1% AuBr₃ failed to find Au incorporated in the crystal above the detection limit of 0.9 ppm wt. This null result was checked by Extended X-Ray Absorption Fine Structure (EXAFS) spectra on powdered single-crystal samples grown with Au in the melt, also failing to find

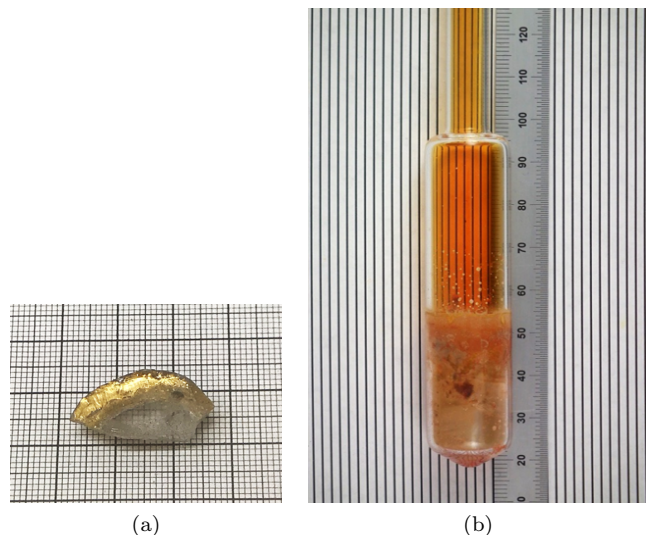


FIG. 1. (a) End portion of a BaBrCl:Au crystal after cutting from the main portion of the grown boule. The piece is covered with a thin layer of metallic gold resulting from AuBr₃ dissociation into elemental gold and bromine (cm/mm grid). (b) Photograph of the ampoule above the crystal grown from a BaBrCl:AuBr₃(0.1%) charge. In this photograph taken prior to opening the ampoule after growth, the orange color is due to bromine gas (Br₂). The smaller diameter tube at top is used for ease of sealing.

Au incorporated into the crystal.

B. Measurement of picosecond absorption

The laser system and the main experimental method have been described in Refs. [26] and [27]. The regeneratively amplified Ti-sapphire mode-locked laser delivers fundamental pulses at 10 Hz, 840 nm, 200 fs. The bandgap of BaBrCl has been reported to be approximately 7.3 eV [25]. Inspection of Fig. 2 along with knowledge of the bandgap confirms that two-photon absorption of the 2.95-eV laser 2nd harmonic pulse would reach a final state only in the transparent impurity edge of BaBrCl, and so will not be useful for an interband pump pulse. The 3rd harmonic (280 nm, 4.43 eV) pump pulses of ~300 fs duration at the sample produce 2-photon interband excitation of hot free carriers in the bulk BaBrCl crystal. The excess kinetic energy of the carrier pairs is 8.86 - 7.3 = 1.56 eV, offering a rough approximation of carrier energies in the phonon-mediated relaxation stage of gamma energy deposition. Judging from Fig. 2, interband excitation of BaBrCl should be the main result of two-photon excitation by the 3rd harmonic laser pulses in both undoped and Au-doped BaBrCl. Two-photon absorption was confirmed by measuring fluence-dependent transmission of the 4.43-eV pump beam, corresponding to the method of Ref. [28].

However, Fig. 2 shows that the Eu dopant present at

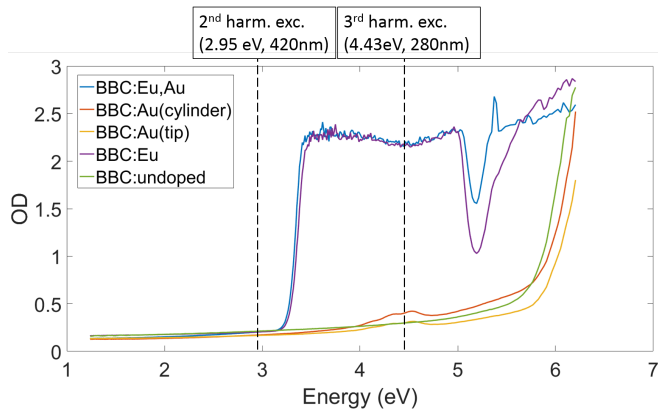


FIG. 2. Absorption spectra of the 5 samples studied before radiation, also indicating the 2nd and 3rd harmonics of the laser pulse. The 3rd harmonic at 4.43 eV can generate electron-hole pairs of total energy 8.86 eV by two photon absorption in undoped and Au-doped BaBrCl, and can produce resonantly enhanced multiphoton excitation as well as direct Eu excitation in Eu-doped samples.

0.5 mole% in our Eu-doped and Eu/Au codoped samples will strongly absorb the 4.43-eV pump pulses. Thus we should view the experiments on all 4 sample doping types as comprised of two possibly separate experiments: One in undoped and Au-doped samples probes absorption clearly induced by interband excitation of hot free carriers in the bulk crystal, and another in Eu-doped and Eu/Au codoped samples probes transient absorption induced by excitation involving one-photon absorption by Eu, possibly as the first step of a resonantly-enhanced multiphoton transition. One possibility for what may be measured in the experiments on Eu-doped samples is that the induced transient absorption spectra will characterize excited europium, Eu^* . We will call this possibility (a). Another possible outcome is that there will be resonantly enhanced production of free carriers. The 3rd harmonic pump pulse energy in our experiment is 20 μJ , corresponding to pulse power of 70 MW and power density (irradiance) at the $\sim 1\text{-mm}$ radius pump spot of $\sim 2 \text{ GW}/\text{cm}^2$. This power density deposits a significant fraction ($\sim 50\%$) of the pump pulse total energy in the 2-mm thickness of undoped BaBrCl by two-photon absorption. With Eu doping at such irradiance, it is likely that Eu will function as a resonant-enhancement intermediate state for two- and three-photon absorption producing mainly hot electrons and holes, i.e. that most of the excited Eu^* produced should be photoionized by the same pulse. Whereas two-photon absorption is dominant via the virtual intermediate states in pure BaBrCl, resonant enhancement can make three-photon absorption dominant alongside two-photon absorption. We have previously found indirect evidence of strong three-photon excitation resonantly enhanced by cerium in $\text{LaBr}_3:\text{Ce}$, in which the outcome was identified by picosecond spectroscopy to be electron-hole pairs relaxed in the form of self-trapped excitons [26]. The process can be approxi-

mately described as absorption of one photon to produce excited Ce^* or Eu^* as the case may be, followed by photoionization of the Eu^* bound excited electron to the conduction band by a second photon, and charge transfer of an electron from the valence band into the Eu^* hole state using a third photon. At the end of this, Eu is left in its electronic ground state, there is some lattice vibration generated, and there is a hot electron and hole sharing excess kinetic energy from the 3 photons absorbed. Note that the resonantly enhanced three-photon absorption can produce electron-hole pairs with up to $3 \times 4.43 = 13.29 \text{ eV}$, i.e. hotter than by two-photon absorption which dominates in pure BaBrCl. We will call resonantly-enhanced two- and three-photon absorption the possibility (b) that may be observed.

We can experimentally distinguish whether possibility (a) or (b) is dominant in the actual measurements. The test will be to observe and identify the initial induced absorption spectrum in the clear case of interband excitation of undoped and Au-doped BaBrCl samples, and then inquire whether the initial induced absorption spectrum in the Eu-doped samples is basically different or substantially the same as in the samples without Eu.

Time resolution of induced absorption in undoped BaBrCl, Au-doped, Eu-doped, and Eu/Au codoped BaBrCl was measured using the pump-probe picosecond absorption technique. By tuning the optical parametric amplifier (OPA) to a specific probe wavelength and varying the arrival time of the pump pulse, we could plot the delay time traces of induced transmission recorded by an amplified PbS detector in the spectral range 1000 to 2900 nm. To cover the red-visible spectral range, the frequency of the infrared OPA output was doubled. The photodetector used in the spectral range from 575 nm to 1100 nm was a silicon detector. The total spectral range covered with the tunable OPA and its direct or frequency-doubled output extended from 575 nm (2.16 eV) to 2800 nm (0.44 eV).

Each different wavelength measured is on a fresh spot of the sample. Before any pump exposure on a given spot, the probe-only transmitted signal (I_0) was measured on the fresh spot, using 300 probe-only pulses averaged. This pristine I_0 value is used as the reference signal to compute transient and residual induced absorption on the selected spot. The induced change of the optical density is calculated by the formula

$$\Delta OD(t) = -\log_{10}\left(\frac{I(t)}{I_0}\right) \quad (1)$$

$I(t)$ is the transmitted signal at time t after the most recent pump pulse exposure. All experiments were conducted at room temperature.

III. RESULTS

A. Stable F_{Cl} and F_{Br} absorption bands induced by electron-hole pair generation in BaBrCl

Each sample was irradiated by the 3rd harmonic laser pulses (4.43 eV photons, two-photon absorbed) at 10Hz, averaging 30 shots for each of 100 delay settings comprising a pump-probe delay scan at a given wavelength. Thus about 3000 pump pulses in 5 minutes exposure were accumulated in acquisition of a time delay trace. In order to assess the residual color center absorption produced, a spot on each sample was exposed to the pump pulses for two minutes at room temperature and then the sample was moved within about 3 minutes to a spectrophotometer for measurement of the optical absorption spectrum. In Fig. 3, the stable defect absorption measured in a Cary 50 UV-visible spectrophotometer after 1200 laser shots exposure is compared for all 4 samples. Only the undoped BaBrCl sample exhibits stable absorption that can be recorded above noise three minutes later in a spectrophotometer. This was backed up by visual observation as recorded in the photograph inset. It shows a purple spot of color center absorption that could be seen for several minutes up to an hour after accumulated interband laser excitation (two-photon absorption - total 8.86 eV) at room temperature. It is visible to the eye only in the undoped sample. Offsets evident in the mostly flat spectra for the doped samples were probably due to differences in surface finish including faint fogging of some of the encapsulated hygroscopic samples. A more sensitive measurement by optically stimulated luminescence (OSL) at room temperature revealed color center bands at about 1.8 and 2.3 eV in a Eu-doped sample as well as the undoped one, but that is undetectable above baseline noise of the transmission spectroscopy employed in Fig. 3.

The most prominent spectral features in Fig. 3 are the two absorption peaks at about 1.83 and 2.3 eV. These can be compared with peaks at 1.83 eV and 2.25 eV in published difference absorption spectra (“after x-ray” minus “before x-ray”) measured in BaBrCl:Eu by Xianguo et al [29]. The 1.8 eV band was identified as F_{Cl} absorption (F center on a chloride site) and the 2.3 eV band as F_{Br} (on bromide site) by Bourret, et al [18] making use of DFT calculations similar to those discussed in Section IV.

B. Time-resolved absorption measured with picosecond laser pulses in BaBrCl without and with dopants

Figure 4 shows time-resolved rise and decay curves of induced absorption at 700 nm (1.77eV), which lies in the low-energy side of the absorption band of an F center on a Cl site, denoted F_{Cl} . The induced change in Optical Density (OD) can be read from the vertical axis. Figure 4 displays data for each of the four different sample doping

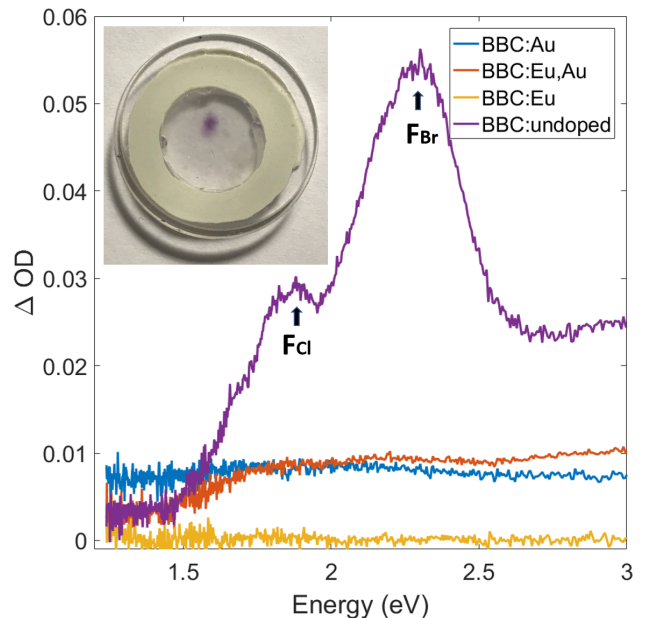


FIG. 3. Residual color center spectra produced by 1200 shots exposure to two-photon interband excitation at 10 Hz, measured by spectrophotometer within ~ 3 minutes of the last shot for 4 samples with different doping conditions. Inset: photograph of the undoped BaBrCl sample, showing purple color in the laser irradiated spot.

conditions. Clockwise from upper left, the BaBrCl samples are undoped, Au-doped (in the melt), Eu-doped, and Eu/Au-codoped (in the melt). The absorption induced by a pump pulse is plotted for relative probe arrival times from $t = -4$ ps to $+16$ ps where $t = 0$ ps corresponds to coincident arrival of the pump and probe pulses. The meaning of negative delay is that the probe pulse arrives before the pump pulse it is paired with, and so probes the effect of the pump in the preceding pair 0.1 s earlier, as well as residual absorption from still earlier pulses at 10 Hz. Each plot represents 100 time-delay values spanning the stated time range, and at each time delay, the signal from 30 pump/probe pulse pairs was averaged.

Look first at the negative-delay feature circled on the undoped BaBrCl response in Fig. 4, which we shall call the “pedestal” of residual absorption. The pedestal rises with a very steep slope at first and then changes to a much lower slope as delay time approaches $t = 0$. Although the horizontal axis is labeled “Time (ps)”, it is really representing accumulated pump-pulse shots received at 10 Hz in the negative-delay region. Thus the pedestal plot registers purely the build-up of induced absorption versus radiation dose measured in units of accumulated pump pulses. This may seem like using an ultrafast sledge-hammer to do a nearly steady-state 100-ms radiation damage experiment, but in fact it is important and useful to see this stage of radiation response registered quantitatively on the same plot with the picosecond transient absorption measured at positive delay. The

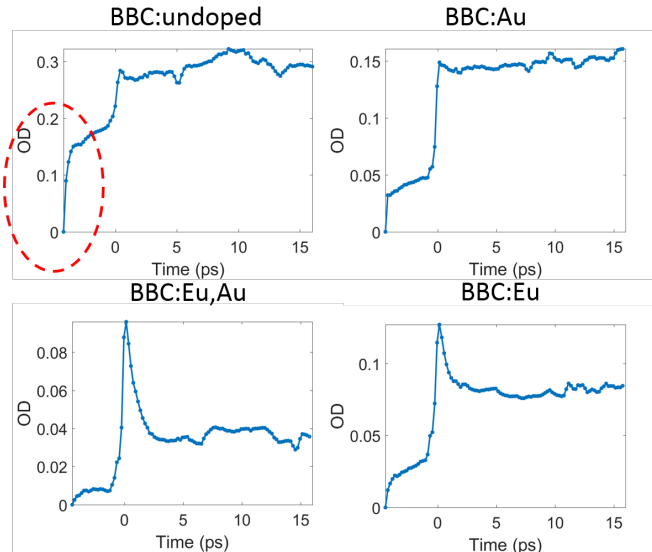


FIG. 4. Time dependence of induced absorption in BaBrCl samples that are (clockwise from upper left) undoped, Au-doped, Eu-doped, and Eu/Au codoped. These measurements are at the wavelength of 700 nm (1.77 eV), which is within the F_{Cl} band. The circled feature registered at negative delay in the undoped sample is the “pedestal” of induced residual absorption, effectively versus accumulated laser shot number as discussed in the text.

steep rise and subsequent saturation of residual F-center absorption in the pedestal region is a phenomenon well-known from the alkali halide literature. The steep initial rise versus dose is often referred to as the “easy stage of F-center formation” in which ionizing radiation produces free electrons that are captured on pre-existing halide vacancies. The shape of the pedestal that we observe closely resembles the growth of the F band under x-ray radiation for alkali halide crystals measured by Rabin and Klick [30]. Saturation occurs when the pre-existing vacancies in the probed volume have all captured electrons. That saturation is followed by the harder “second stage” of F center production in which one actually creates new vacancy-interstitial pairs (F center + H center pairs), with the residual 100-ms survivors having a shallow slope versus dose.

The easy formation of F centers by electron capture on pre-existing vacancies might impact scintillation performance, e.g. by removing electrons from the recombination pool that could otherwise contribute to light emission. A quick conclusion that appears just from inspection of the negative-delay region in Fig. 4 is that the pedestal of easy F-center formation by populating old vacancies is largest in the undoped sample, next largest in the Au-doped, yet smaller in the Eu-doped, and smallest of all in the Eu/Au co-doped. The stable (~ 3 minutes) F centers were only formed appreciably in undoped BaBrCl, and not observable in any of the doped samples. In contrast, the 100-ms surviving F centers contributing to the pedestal in Fig. 4 can be observed in all samples,

with the amount of suppression depending on doping.

Next, consider the positive delay portion of the data in Fig. 4. When the probe pulse is at a positive delay relative to the pump, it measures the change in transmittance produced by the associated pump pulse that arrived just a few picoseconds earlier, as typically understood in pump-probe experiments. This produces the big vertical jump at $t = 0$ ps delay for all four samples shown. The picosecond pump-induced signal rides on top of the pedestal, which therefore serves as a “recent baseline” for all positive delays.

Comparing the undoped and Au-doped plots in the top row of Fig. 4, the response at positive delay is similar for both samples. It is a sharp step up from the saturated pedestal, rising from 10% to 90% in about 300 femtoseconds. This corresponds to the duration of the amplified pump pulse, implying a very fast rise of induced absorption. The rise is followed in the undoped and Au-doped samples by an initial fast decay of $< 10\%$ in amplitude followed by flat or slightly rising absorption out to 16 ps. The height of the fast rise up from the pedestal at $t = 0$ ps is approximately equal ($\Delta OD \approx 0.1$) for both the undoped and Au-doped samples. From these data, the effect of the Au doping seems mainly to be a suppression of the “easy F center” pedestal from $\Delta OD \approx 0.18$ in undoped to 0.048 in Au-doped. The simplest way to achieve this would be if putting AuBr₃ in the melt suppresses bare halide ion vacancies, including Cl⁻ vacancies singled out simply because we are looking at the F_{Cl} wavelength in Fig. 4.

Now look at the Eu-doped and Eu/Au-codoped samples in the bottom row of Fig. 4. The size of the fast rise above the pedestal level at $t = 0$ ps is still about the same, $\Delta OD \approx 0.1$, as in the undoped and Au-doped samples. Most noticeable is that in both samples containing Eu there is a very rapid (~ 1 ps) decay from the maximum induced absorption just after $t = 0$ ps. The rapid rise and decay appears as a spike of absorption at $t \geq 0$ ps. Since Fig. 4 monitors absorption in the region of the F_{Cl} band, one might try to interpret the fast spike of absorption just after the pump pulse in the two samples containing Eu as additional absorption from some Eu charge state produced on top of normal F centers. However, the “on top of” supposition doesn’t work because the 10 ps plateau with Eu present is much lower than the 10 ps plateau absorption of F centers in both of the non-Eu crystals in Fig. 4. Supposition of an induced Eu charge state in competition with F center production doesn’t make good sense either, because the supposed Eu state absorption drops by up to 70% in about 2 picoseconds. One would be losing too many Eu excited states to be consistent with the good light yield of this material, which for 5% Eu doping achieves 55,000 photons/MeV or almost 100% of theoretical maximum light yield based on estimating invested energy $2.5E_{gap}$ per electron-hole pair with $E_{gap} \approx 7.3$ eV. We will temporarily refer to the fast-decaying spikes in Fig.4 as “Eu attacking the induced 700 nm absorption”, and then try to assign the

absorption and the attack mechanism after considering the spectrum of induced transient absorption.

The effect of the dopants on the induced absorption at 700 nm if attributed to F_{Cl} -like defects can be summarized in four observations:

(1) The undoped BaBrCl exhibits the largest pedestal of residual F_{Cl} -like defect absorption. A prompt further rise of F_{Cl} -center absorption at $t = 0$ ps (pump-probe coincidence) occurs on top of the pedestal of accumulated residual absorption. This steep rise at $t = 0$ ps represents new F-H defect pairs created together from the perfect lattice. On the picosecond time scale of Fig. 4, one cannot tell if they persist, but they are mostly transient based on the slope of the pedestal's hard stage. Since 30 shots were averaged at each increment of 0.2 ps in delay time, we divide the absorption accumulated during the hard stage of the pedestal in undoped BaBrCl, $\Delta OD \approx 0.04$, by the ~ 480 accumulated shots comprising that part of the pedestal. Then the induced residual F-band ΔOD in the hard stage is roughly 10^{-4} per shot in undoped BaBrCl. Compare this to the vertical rise of induced transient F-band absorption which is seen in Fig. 4 to be $\Delta OD \approx 0.1$ per single shot. This is reminiscent of results from transient absorption spectroscopy in alkali halides, particularly KCl and KBr [31].

(2) Doping with Au in the melt suppresses the pedestal of easy F centers to about 30% of its undoped value, but seems to do little else. In particular, Au does not “attack” the 700 nm absorption the way that Eu does.

(3) Doping with Eu suppresses the pedestal of easy F centers to about 20% of the undoped pedestal value, and it quickly “attacks” the fresh 700 nm absorption induced by the pump pulse.

(4) Codoping with Eu and Au has a similar effect on 700 nm absorption as doping with Eu. The easy F pedestal is suppressed to about 5% of the undoped pedestal and the attack on 700-nm induced F_{Cl} -center absorption appears to be the most complete with codoping, i.e. reduction to about 32% of the maximum above pedestal background within 2 ps.

The above measurements and analysis were repeated for other wavelengths across the spectral range accessible to our OPA and frequency-doubled-OPA, from 2800 nm (photon energy 0.44 eV) to 575 nm (photon energy 2.16 eV). The characteristic time profiles already introduced in Fig. 4 occur and change in a fairly systematic way versus probed photon energy. Figure 5 presents data for 575 nm (2.16 eV), which is spectrally within the low energy side of the F_{Br} defect band.

The same general discussion given above of the induced 700 nm absorption versus doping applies as well to the 575 nm absorption (2.16 eV) in the F_{Br} band region. The pedestal of easy residual F-center formation by electron capture on old vacancies is even higher in this F_{Br} region, consistent with the relative heights of stable F_{Br} and F_{Cl} defects measured by spectrophotometer in Fig. 4. Notice in both F-center wavelengths that when either Au or Eu is added, the negative delay pedestal of “easy”

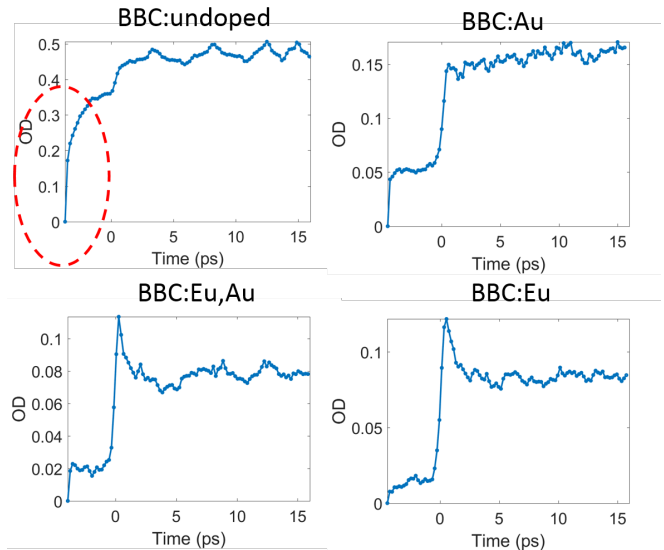


FIG. 5. Induced absorption time dependence curves measured at 575 nm (2.16 eV), F_{Br} band region.

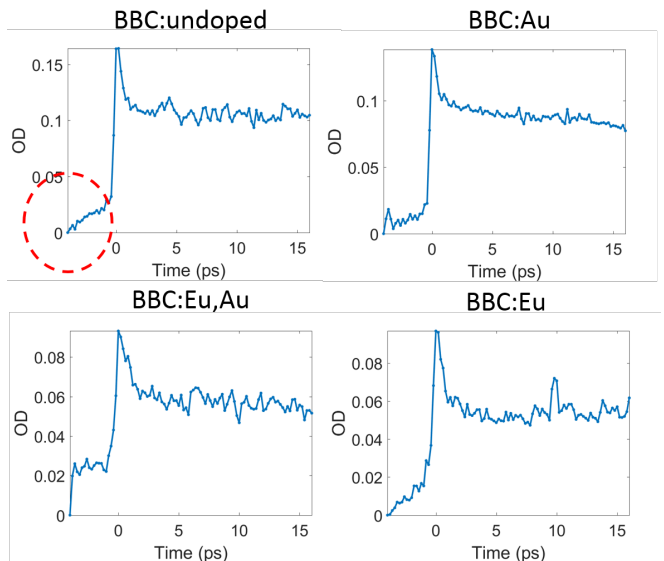


FIG. 6. Time dependence of induced absorption measured at 1200nm (1.03 eV).

F formation is reduced.

The attack by Eu on the 575 nm absorption associated with F_{Br} is not as strong as it was on 700 nm absorption associated with F_{Cl} . Whereas Au codopant seemed to assist the attack of Eu on the F_{Cl} absorption at 700 nm (Fig. 4), Au does not obviously assist the attack of Eu on the F_{Br} absorption at 575 nm (Fig. 5).

Figure 6 shows time profiles at a probe wavelength of 1200 nm (photon energy 1.03 eV) that is out of the spectral range of either the F_{Cl} or F_{Br} defect bands. Yet it exhibits significant transient absorption induced by interband excitation. The entire rise and decay traces

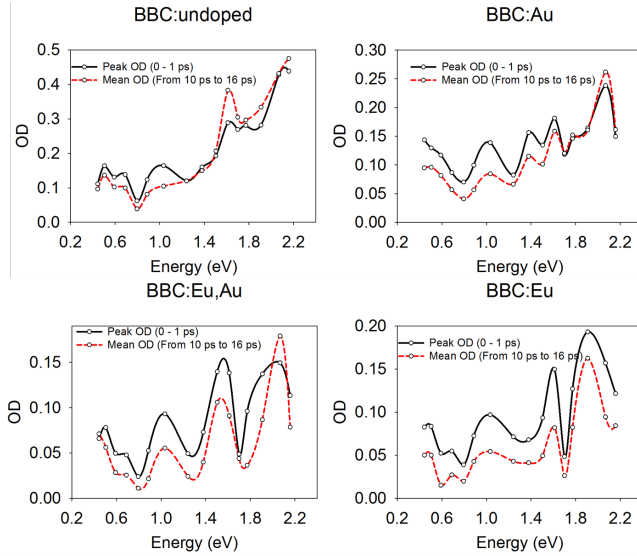


FIG. 7. The induced absorption spectra for the $0 < t < 1$ ps peak in black, and the $10 < t < 16$ ps plateau in red dashed, for each of the BaBrCl doping choices labeled.

for this wavelength appear almost identical regardless of doping, suggesting that the band at 1200 nm is a universal property of the BaBrCl host. 1200 nm is the peak of a transient induced absorption band that we will suggest is Type II STE, using terminology from alkali halides. The “attack” of induced absorption at 1200 nm cannot be attributed to Eu in this case. It is more general, independent of dopant type or doping at all. We suggest it could be nonlinear quenching of the type II STE at densities of order 10^{18} cm^{-3} needed to record reasonable optical absorption in this experiment.

C. Transient absorption spectra - Defect bands and STE

Next, we show spectral plots constructed from time-dependent absorption data at multiple wavelengths. Figure 7 plots the induced absorption spectra for the maximum absorption occurring in $0 < t < 1$ ps in black, and the plateau value of absorption averaged from 10 to 16 ps in red dashed lines, for each of the four doping conditions. The spectral density of the measurement points is relatively sparse because of the need to use a fresh spot of the sample for each wavelength. Even so, one can recognize a commonality of four induced absorption bands that seem to be shared by all samples despite different doping choices. The time-dependence traces reviewed earlier pointed to distinct differences in rise and/or decay characteristics versus doping. In contrast, the spectra point more to similarities in spectral shape common to all samples without much regard to doping. This suggests that the main four spectral bands are characteristic of BaBrCl itself rather than of particular dopants.

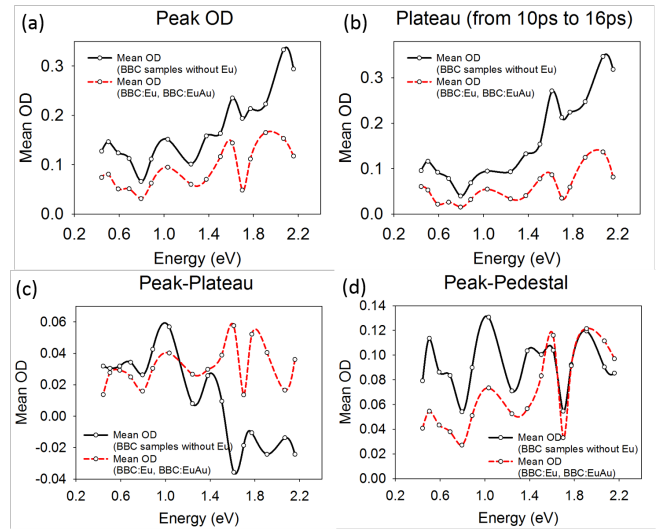


FIG. 8. Induced absorption spectra are averaged for all BaBrCl samples without Eu doping (black) and for all BaBrCl samples with Eu doping (red dashed), for the maximum absorption achieved in $0 < t < 1$ ps in upper left, and averaged absorption in the plateau defined as $10 < t < 16$ ps in upper right. Difference spectra are presented in the lower row. Using terms defined in the text, the difference spectra are (Peak - Plateau), and (Peak - Pedestal).

To highlight the features independent of doping and improve signal-to-noise, Fig. 8 averages the induced spectra for all three samples without Eu (i.e. undoped, Au-tip, and Au-cyl) plotted in black, and spectra for samples with Eu (i.e. Eu-only, Eu + Au codoped) plotted in red. The top row plots spectra of the peak OD ($0 < t < 1$ ps) and of the OD persisting in the plateau averaged from 10 to 16 ps. In the top row, induced absorption at peak and plateau is measured relative to the pristine-sample reference I_0 as described in Section II.B, Eq. (1), so the plotted OD spectrum includes the “pedestal” of residual F center absorption induced by all previous shots.

The bottom row of Fig. 8 plots the difference spectra, “Peak - Plateau” and “Peak - Pedestal”. Both of these difference spectra exclude the pedestal of residual F centers. In Fig. 8(d), Peak - Pedestal, the general rise toward high photon energy associated with the pedestal is eliminated, and the four induced absorption bands common to all sample dopings are revealed as having comparable strength at ~ 1.9 eV, 1.6 eV, 1.0 eV, and ~ 0.5 eV. Fig. 8(c) confirms our observation that the Peak - Plateau difference, earlier called “attack on induced F band absorption by Eu dopant”, is confined mainly to the bands at ~ 2.0 and 1.6 eV. It will be noted that the list of the 4 absorption band peaks just given does not include the two F-band peaks at 1.83 and 2.3 eV known from stable spectra. The picosecond total absorption spectra for both the peak (< 1 ps) and plateau (~ 10 ps) features have “F-like” bands at ~ 2.0 eV and 1.6 eV, in each case about 0.2 eV lower than the known stable F_{Br} and F_{Cl} peaks.

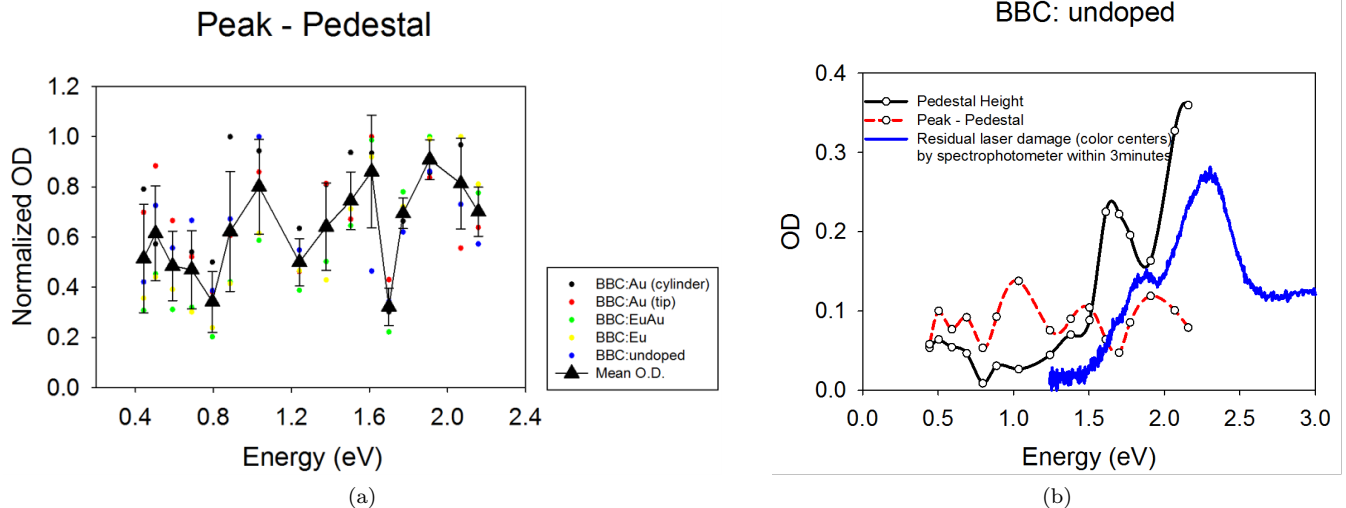


FIG. 9. (a) Transient induced absorption (Peak-Pedestal) for five different samples normalized at the maximum optical density of each spectrum are shown by small circular points color coded in the legend. Their mean value at each wavelength is shown by large triangular points with bars representing one standard deviation above and below the mean. The mean values are connected by straight-line segments. (b) Spectra of stable F-band absorption after ~ 3 minutes (blue noisy curve), pedestal height due to saturated residual F centers measured after at least 100 ms (black), and the difference curve, Peak minus Pedestal, due to newly created F centers within 1 picosecond after the pump pulse (red dashed) in undoped BaBrCl.

Although Fig. 7 is suggestive of four peaks common to spectra of all of the differently doped samples, the spectral resolution in each data set is poor due to the sparse points, and so we examine whether the suggested peaks are significant relative to variance in multiple measurements taken on different sampled spots at each wavelength. We have data in the same spectral series on a total of five different samples: undoped, Au-doped from the tip of the boule and Au-doped from the cylinder part of the boule, Eu-doped, and Eu/Au codoped. To examine if there are spectral peaks characteristic of the host BaBrCl rather than the dopants, we have averaged data for all 5 samples and computed the standard deviation at each wavelength, shown as error bars representing one standard deviation above and below the average in Fig. 9(a). In addition to display of the error bars, the five separate measurements are shown as small circular points identified by color with respective sample dopings. The average value at each wavelength is a larger triangular point and they are connected by straight line segments as a guide for the eye. The variance represents not only statistical noise, but also differences from doping and location on the crystal boule or sample surface. In any case it represents an upper limit of the noise among five samples. The quantity plotted is Peak minus Pedestal normalized OD using the definitions of those terms already given. The difference plot eliminates the pedestal of residual F-center absorption which changes continually during a multi-shot measurement especially in the undoped sample and is not the transient induced signal of interest. The spectra for different samples were normalized at their maximum OD before averaging.

The four peaks in Fig. 9(a) exceed the standard deviation at each respective peak by factors of 11, 3.8, 3.8, and 3.3 from high energy to low. The peak-to-adjacent-valley difference divided by the mean peak-and-valley standard deviation gives ratios of 6.9, 3.6, 2.0, and 1.2 in the same order. These ratios support the conclusion that the peaks are real relative to noise and furthermore that the surviving peaks characterize properties of the host BaBrCl rather than particular properties of the dopants.

In Fig. 9(b), the red dashed, black, and blue-noisy spectra represent absorption characteristic of about 1 picosecond, 100 milliseconds, and 3 minutes after the latest pump pulse that generated electron-hole pairs. There are three F-band-like pairs of absorption peaks in Fig. 9(b), each shifted spectrally from the others. The noisy blue spectrum shows the stable F_{Br} and F_{Cl} absorption bands with peaks at 2.3 and 1.83 eV. The black spectrum is that of metastable F-like centers registered in the pedestal, formed as little as 100 milliseconds after e-h pair generation. Recall from the discussion in Section III.B that the pedestal is measured at negative probe-pump delay, where the probe measures effects of the pump pulse in the previous pulse pair 100 ms earlier, along with residual effects of prior pulse pairs. The pedestal spectrum is shifted about 0.2 eV to the low energy side of the stable peaks. By analogy to alkali halide studies [31], these could be F centers perturbed by proximity to interstitial H centers created at the same time. These metastable perturbed F centers must exist for up to 100 msec to be observed as residual. The red dashed spectra of (Peak - Pedestal) in Fig. 9(b) have a large ~ 0.4 eV shift to the low-energy side of the stable F bands, i.e. peaks at 1.95

and 1.5 eV, and may be regarded as highly perturbed F centers in a close F-center/H-center pair. It was shown first in alkali halide studies that a nearest-neighbor F-H vacancy-interstitial pair has significant overlap of the F-center electron with the H-center hole and thus behaves as a lattice-relaxed electronic excited state of the crystal, an off-center self-trapped exciton[32]. In preparation for further discussion of relaxed electronic excited states in BaBrCl and as background for some use of analogies and nomenclature from the alkali halides, we present in the following section electronic structure calculations of self-trapped excitons and defects in BaBrCl.

IV. ELECTRONIC STRUCTURE CALCULATIONS OF SELF-TRAPPED EXCITONS AND DEFECTS

We performed first-principles electronic structure calculations as a guide for interpreting observations on transient absorption induced by electron-hole pair production in BaBrCl. Many detailed experimental studies using specialized techniques have been used to construct what is now a reasonably complete understanding of STEs and their conversion to F-H defect pairs in alkali halides, including optically-detected electron paramagnetic resonance [33], electron-nuclear double resonance [34], polarized spectroscopy with oriented self-trapped holes and self-trapped excitons [35], time-resolved absorption [36], experiments conducted on mixed crystals [37], and under applied stress [38]. While STE phenomena have continued to be discovered in additional materials through the present day, no other material has received the attention of so many experimental techniques focused on its STE properties as alkali halides, except possibly SiO₂ due to its technological importance. Instead, recently developed electronic structure calculations with demonstrated ability to capture the features of exciton and hole self-trapping offer an economical tool often used to explore relaxed excited states, polarons, and defect formation in newly considered materials. We summarize here the results of electronic structure calculations on self-trapped excitons and some relevant defect properties in BaBrCl. Similarities of structure and properties to self-trapped excitons in alkali halides will be pointed out.

At low temperature the crystal structure of BaBrCl is orthorhombic (space group $Pnma$). This is the same structure as BaCl₂, BaBr₂ and BaBrI, while BaBrF is tetragonal (space group $P4/nmm$). The relation between BaCl₂ and BaBr₂ and the mixed halide structures is that BaCl₂ and BaBr₂ have two inequivalent halide sites so that in the mixed halides the larger and smaller halide ions occupy different sites. This also means that in BaBrI, Br is the smaller halide ion and occupies a different site from BaBrCl where it is the larger halide ion.

We have performed first-principles electronic structure calculations with the VASP [39, 40] and CP2K [41, 42]

codes. The VASP code was used for bulk band structure and defect level calculations using the PBE generalized gradient approximation (GGA) functional while the CP2K code was used for PBE0 hybrid functional calculations for V_k center and STE calculations. The CP2K code has the advantage with its mixed basis Gaussian and plane waves that it has a very efficient implementation of hybrid functionals allowing us to easily simulate systems of hundreds of atoms required to accurately model the atomic relaxation of the V_k center and corresponding STE states. The GGA functional does not correctly model the V_k center and more advanced methods such as hybrid functionals are required. More detailed explanations of these calculations along with more extensive results will be the subject of a future publication.

The first calculations we performed were using the VASP code for band structure calculations of BaBrCl and BaBrCl with Br and Cl vacancies. We used cell sizes of 192 atoms and the PAW approach with the PBE functional and pseudopotentials. The halide vacancy calculations were performed by removing one halide from the supercell and relaxing the atomic positions, with the cell size fixed at the bulk structure, until the forces on each atom are below 0.01 eV/Å. The vacancy states have a hydrogen-like character modified by the lattice structure so the Cl vacancy state is a distorted 1s state. The depth of the Cl vacancy state below the CBM is 0.45eV while the Br vacancy state is 0.4eV below the CBM. By purely energetic arguments the Cl vacancy state would then be a stronger electron trap than the Br vacancy state and more likely to form. In relation to the absorption experiments in Section IIIC we also looked at the excited states of the halide vacancy F-centers. As mentioned earlier the excited states of the F-center tend to be hydrogen-like and like the 1s character ground state are very localized. We can therefore scan up through the empty states above the Fermi level to find the excited states associated with the F-centers. The first excited state has a distorted 2s type character. We then calculated the energy difference between the empty first excited state and the 1s ground state to have some measure of the absorption energy of the two different F-centers. While this is a very approximate way to calculate the absorption energy of the F-centers it gives some measure of the ordering of the absorption energies of the two F-centers. We found that the difference in energy between the excited state and ground state of the Cl and Br F-centers was 1.8eV and 2.1eV in remarkably good agreement with the experimental results of 1.83eV and 2.25eV and helping to identify which absorption is associated with which halide F-center. This also places the excited states of the two F-centers in the conduction band.

The next step in our calculations was to look at the formation of V_k centers and corresponding STEs using a constrained occupancy approach with hybrid-functionals using the CP2K code. To perform these calculations we again take a large supercell based on the bulk structure, then move two halide atoms closer together and remove

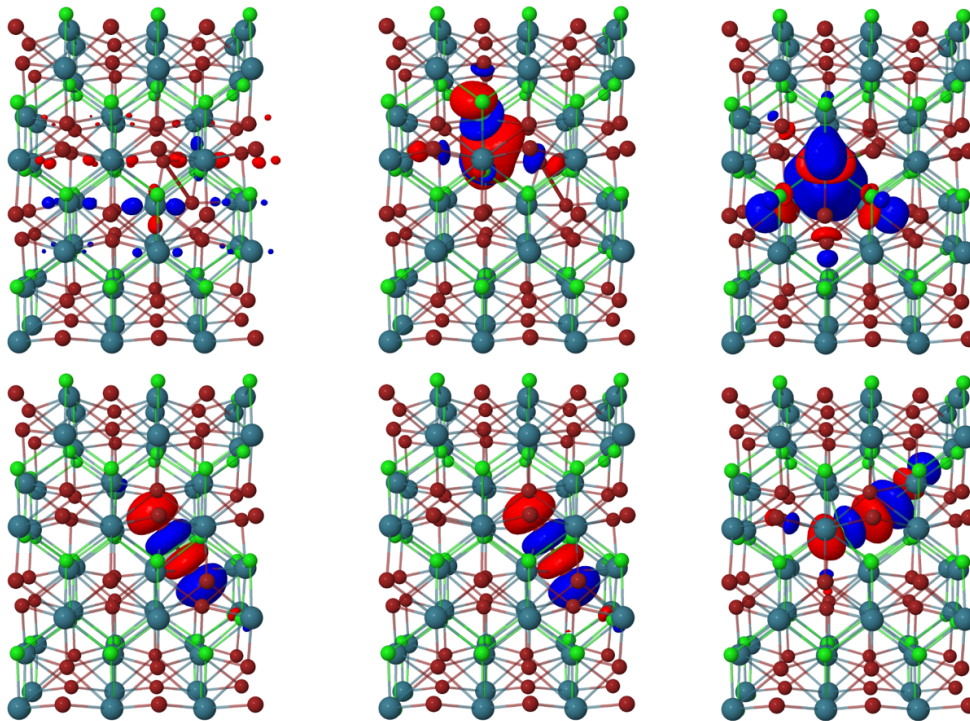


FIG. 10. Charge-density isosurfaces from left to right: Type I, II and III STEs in BaBrCl. Top: electron states, Bottom: hole states.

an electron to form a self-trapped hole. An atomic relaxation is then done on the cell to obtain the equilibrated V_k center geometry. In order to model an STE we constrain the system to be in the excited triplet state by blocking the number of electrons in one of the spin channels to be larger than in the other spin channel, this time performing the calculation on a neutral cell. As previously mentioned there are typically three types of STE relaxations in halide materials [32]. For alkali halides, type I has a geometry close to the V_k center geometry where two halide atoms move symmetrically together and the hole and electron state are centered on the two halide atoms. In type II, one halide moves closer to the neighboring halide which remains at the bulk lattice site. In type III, a halogen atom moves through to a neighboring unit cell creating an interstitial and leaving a vacancy (Frenkel type defect). Type III can be thought of as an F-center and an H-center pair. In the case of the binary alkali halides the crystal structures are primarily face-centered cubic and some body-centered cubic so there is only one unique geometry of a halide pair for forming the three types of STEs. In the case of BaBrCl since it has two types of halides and an orthorhombic crystal structure the situation is more complicated. There are seven possible halide pairs geometries for this crystal structure consisting of pairs of Cl-Cl, Cl-Br and Br-Br pairs. If they can all form type I, II and III STEs then there are twenty one different possible STE geometries. We have not done an exhaustive study of the stability of all possible STE geometries in BaBrCl, but examples of

the most stable type I, II and III geometries we found are shown in Figure 10. From a theoretical point of view we find that these types of STEs are stable in a similar way to the alkali halides and LaBr_3 . Further studies we did were to investigate the migration of these types of STEs as well as properties of hole and electron traps. We performed these calculations via molecular dynamics simulations at high temperature of the exciton states to determine migration pathways and then used the nudged elastic band method to determine the migration energy barriers. While we found the migration pathways can be rather complex moving between the different types of stable STEs, the energy barriers to migration are typically of the order of 0.1 eV. Thus the STEs are mobile at room temperature and can easily migrate to the activator. The timescale for the STE to move to a neighboring site is of the order of picoseconds at room temperature. We also studied the migration of H-center hole traps associated with interstitial halides that can be formed from gamma rays via creation of F-H center pairs. Again we found the energy barriers for migration of H-centers to be of the order of 0.1 eV. More details of these calculations will be presented in a future publication.

V. DISCUSSION

A. Self-trapped excitons and other transient defects in BaBrCl

Our measurements of excitation-induced transient absorption spectra in undoped BaBrCl as well as the doped samples (Figs. 7-9) revealed four main spectral bands, at about 0.5 eV, 1.0 eV, 1.6 eV, and 1.9 eV. First principles electronic structure calculations presented in this work find that many of the STE relaxed excited state characteristics now familiar from alkali halides and alkaline earth halides are also predicted for the alkaline earth mixed halide BaBrCl. This included finding relaxed configurations of STEs similar in some regards to those previously labeled in alkali halides as Type I, II, and III (on-center V_k -like, moderately off-center incomplete F-H pair, and strongly off-center nearest-neighbor F-H pair). With the expectation thus supported for finding STE spectra in BaBrCl that seem to follow patterns established in the alkali and alkaline-earth halides, we have suggested that the 0.5 eV band in BaBrCl is the type I STE. The 1- eV band is proposed as Type II, and the 1.6- and 1.9-eV transient bands are attributed to Type III STEs involving partially formed chloride and bromide ion vacancies respectively. The hybrid-functional DFT calculations used in this study cannot predict the STE excited-state transition energies, but have predicted the relaxed STE configurations that underpin the qualitative optical transition assignments suggested above.

The absorption signatures of these relaxed STE states appear in undoped BaBrCl within the laser pulsewidth of 300 fs, and that seems to be the extent of excited states that can be detected within the 0.45 to 2.16-eV spectral range probed in our experiment, aside from the pedestal of residual F-band absorption discussed previously. In terms of spectral bands of transient optical absorption produced, the doped samples seem to behave similarly to undoped. Thus, based on observations within our spectral range, it appears that on the time scale of 1 picosecond, the main form of deposited energy from multiphoton nonresonant or resonant interband absorption is self-trapped excitons.

B. Energy Transfer from STE to Eu in BaBrCl:Eu

Based on the experimental result that the initial pulse-induced absorption bands in Eu- doped samples are similar to the bands already identified as STE in undoped BaBrCl, we conclude that interband electron-hole pair excitation and subsequent rapid relaxation to STE relaxed states is the common starting point in our experiment, whether Eu is present or not. When present, the Eu acts as a resonant intermediate state for multiphoton interband excitation at the 2 GW/cm² pump irradiance used. One of the goals for undertaking the present study of picosecond transient absorption was to seek informa-

tion on the mechanism of energy transfer from electron-hole pairs in the BaBrCl host to the Eu dopant ions.

As previously noted, we do not observe a direct signature of Eu* excited states in the transient absorption spectrum from 0.45 to 2.16 eV. In studies of LaBr₃:Ce by similar technique, we did find an induced absorption signature of Ce* attributed to photoionization of the excited electron to the conduction band at an energy of 2.1 eV . Because the band gap of BaBrCl is wider than that of LaBr₃ (7.3 vs 5.9 eV), it may be that the similar photoionization transition exceeds the 2.16 eV limit of our OPA probe. A distinct effect that is observed in our spectroscopy is the rapid “attack” on induced absorption in the Type III STE bands (1.6 and 1.9 eV) when Eu is present, and only then. We suggest that this rapid loss of STE population in the presence of Eu is due to energy transfer from STE to Eu, since the 40% loss in STE population would otherwise contradict the light yield of BaBrCl:Eu, which is near the theoretical maximum if $\beta E_{\text{gap}}=2.5E_{\text{gap}}$. We cannot rule out that some Eu* may also be produced by the laser pulse since Eu* absorption seems invisible in our spectral range. However, we also observed that the strength of induced STE absorption at $t \approx 0$ ps in 0.5% Eu-doped BaBrCl is about the same ($\Delta OD \approx 0.1$) as in undoped BaBrCl. This implies that most of the interband excitations result in STE even in Eu-doped crystals, and that energy transfer from STE to Eu* should be regarded as the main route to populating Eu* in BaBrCl:Eu.

Given the observed ~ 1 picosecond time for the “Eu attack” attributed to energy transfer from STE to Eu* , dipole-dipole transfer at nearest-neighbor distance seems the likely mechanism. In LaBr₃:Ce, the 1-ps dipole-dipole transfer time was encountered only in the case when the excitation pulse involved resonant excitation by Ce dopant so that the electron-hole pairs were produced adjacent to Ce [26]. When a laser harmonic that avoided resonant absorption on Ce was used, the transfer time was observed on the slower scale of 69 ps at 4.4% Ce doping, attributed to dipole-dipole transfer averaged over a spread of distances falling within the R_{dd} transfer range, which is typically on the order of 3 nm. As discussed in Section II, we do not have the experimental option of avoiding Eu-resonant interband excitation in BaBrCl:Eu, and thus have observed only the transfer from STE to nearest-neighbor Eu. The transfer time was found to be about 1 ps.

Dexter calculated 1-ps dipole-dipole transfer time at nearest-neighbor separation in NaCl under the assumption of good overlap of the emission and absorption band spectra [43]. The dipole-dipole transfer rate is proportional to the overlap of donor emission and acceptor absorption spectra. In BaBrCl, the STE emission band identified by Shalapska et al is broad and centered at ~ 5 eV. The Eu absorption spectrum of BaBrCl:Eu in Fig. 2 extends up to 5 eV and thus overlaps the low energy side of the STE emission band. Our transient absorption spectra show that the effect of “Eu attack” (being at-

tributed to dipole-dipole transfer) is significant only for the two Type III STE bands at about 1.6 and 1.9 eV, not for the Type I and Type II STE bands. In alkali halides, the highly relaxed Type III STEs always have the largest Stokes shift of luminescence among the possible STE configurations [32]. Attributing the low-energy (4.5 - 5 eV) luminescence to Type III STEs in BaBrCl, we may suppose that Type I and II STE luminescence occurs at still higher energy (5 - 6 eV?), out of resonance with Eu absorption. Pushing this interpretation of the STE spectrum in Ref. [25] beyond what the authors intended, we note that it appears as a three-component luminescence band, and only the low-energy component has good overlap with the Eu absorption spectrum.

VI. CONCLUSIONS

Our data have indicated that Au doping does not make a noticeable difference in any of the picosecond time-resolved experiments, except in affecting the size of the pedestal of residual F-band absorption. It suppresses the pedestal of residual F centers, implying that it reduces the concentration of pre-existing halide vacancies that can capture electrons to form “easy stage” residual F centers comprising the pedestal. A likely effect of bare halide vacancy concentration on scintillation would be as a competitor for the electron in radiation-produced e-h pairs that could otherwise contribute to light emission. If one or both of the F_{Cl} and F_{Br} centers formed from pre-existing vacancies hold on to trapped electrons for significantly longer than the Eu^* lifetime, there would be a shift of scintillation decay time toward long-tail emission or afterglow. Such components that exceed the shaping time are not counted in pulse height analyzers. A plausible hypothesis for the beneficial effects of Au codoping to both increase light yield and decrease slow decay is that Au suppresses the concentration of pre-existing halide vacancies, thus decreasing the drain on prompt electron-hole recombinations. This conclusion is similar to that reached by Shalapska et al based on measurements of light yield and afterglow fraction[25].

Our experiments have shown that Eu doping is even more effective than Au doping in suppressing the residual F center pedestal. Furthermore, taking into account both Figs. 4 and 5, we concluded that Au co-doping in Eu-doped crystals does not consistently suppress the pedestal more than Eu doping alone. Can these observations still be consistent with the basic hypothesis suggested above, that Au suppresses the competing halide vacancy electron traps even in Eu-doped crystals? Postulate that the effect of Au doped in the melt is to suppress halide ion vacancies. While Eu (0.5%) is observed to be even more effective than Au (0.1%) at suppressing the pedestal, we will not assume that iso-valent Eu^{2+} operates in the same way as aliovalent Au^{3+} to affect the residual F pedestal. In the literature on storage phosphors, an F center close to a hole captured on or com-

plexed with a Eu ion may contribute its electron by tunneling or thermal release to combine with a hole associated with Eu, resulting in the Eu^* luminescent state.

The essential point is that tunneling recombination of F + Eu close pairs gives suppression of the residual F center pedestal that depends on Eu concentration. This suppression mechanism by Eu doping does not imply that the isovalent Eu^{2+} suppresses the concentration of halide ion vacancies. *That is, Eu^{2+} and Au^{3+} can separately achieve F-center pedestal suppression by different and independent actions. In this hypothesis, the Eu^{2+} suppression mechanism acts on the longevity of the F centers after they are formed, whereas the Au^{3+} suppression mechanism prevents the formation of the “easy F centers” in the first place by eliminating pre-existing halide vacancies that can trap electrons.*

Shalapska et al previously concluded “... that the addition of Au in this material leads to a lower probability of charge carrier trapping at defect sites.” The stated conclusion of Shalapska et al left it open as to “... whether the lower trapping probability is related to a general reduction in the concentration of defects or to a modification of the electron/hole migration and transfer processes in favor of charge carrier recombination on the luminescent centers.” Our time-resolved data and the mechanism suggested above support the first part, that Au doping makes a general reduction in the concentration of halide ion vacancies. Furthermore, conclusions from our time-resolved experiments go on to specify that the second possibility in the two-part conclusion by Shalapska et al is linked directly to the first. Removing halide vacancies and their effect in breaking up electron-hole pairs created by ionizing radiation suppresses the slow STH migration and tunneling transfer processes to the benefit of rapid STE formation followed by picosecond-scale dipole-dipole transfer to Eu.

There is a related issue of what happens to the holes in undoped BaBrCl to allow meta-stability of the residual F centers in the face of possible F-H recombination. For guidance on this, we can go to the alkali halide literature on F and H centers at various temperatures. The H centers are known to be very mobile at room temperature and considerably below, so they are moving rapidly. It was shown that the H centers clump into larger aggregates of multiple H centers, from di-H centers (labeled V_4 centers) [44] up to larger clusters[45] and dislocation loops [46]. These are relatively stable at room temperature and soak up a lot of H centers in specific aggregates, which therefore are trapped at considerable distance from F centers that remain more uniformly distributed.

The hypothesis we have described supposes that Au doping prevents in some way most of the pre-existing halide vacancies that could support easy F-center production. Notice that for this action, the Au doesn't actually have to be present in the crystal at the time of ps spectroscopy and/or scintillation! It may have exerted its effect chemically in the melt. This is important because GDMS and EXAFS measurements indicated that very

little Au is incorporated from the melt into the sample. Then how can Au doping exert control over pre-existing halogen vacancies?

A likely mechanism is that introduction of AuBr₃ in the growth ampoule enriches the melt in Br- anions relative to stoichiometric BaBrCl, suppressing anion vacancies [25]. Another possibility is scavenging of impurities by Au³⁺ in the melt. Monovalent alkali ion impurities substituting for Ba²⁺ in BaBrCl would appear negative because of the Madelung potential on the site occupied and could be charge-compensated by halide vacancies. Since Au³⁺ on a Ba²⁺ site appears positive, it may associate in the melt with effectively negative substitutional alkali cations or substitutional divalent carbonate anions in BaBrCl, for example. Segregation of Au at the growth

interface could eliminate the impurity pair. We have not yet determined which of the possible AuBr₃-related mechanisms is responsible for the halide vacancy suppression that our absorption measurements have indicated.

ACKNOWLEDGMENTS

This work was supported by the US Department of Energy/NNSA/DNN R&D (LB15-ML-GammaDetMater-PD3Jf) under contract No. AC02-05CH11231. The portion carried out at Wake Forest University was under subcontract from Lawrence Berkeley National Laboratory.

-
- [1] M. S. Alekhin, J. T. M. De Haas, I. V. Khodyuk, K. W. Krämer, P. R. Menge, V. Ouspenski, and P. Dorenbos, “Improvement of γ -ray energy resolution of LaBr₃: Ce³⁺ scintillation detectors by Sr²⁺ and Ca²⁺ co-doping,” *Applied Physics Letters* **102**, 161915 (2013).
- [2] E. V. van Loef, C. M. Wilson, N. J. Cherepy, G. Hull, S. A. Payne, W. Choong, W. W. Moses, and K. S. Shah, “Crystal growth and scintillation properties of strontium iodide scintillators,” *IEEE Transactions on Nuclear Science* **56**, 869–872 (2009).
- [3] N. Cherepy, S. A. Payne, S. Asztalos, G. Hull, J. Kuntz, T. Niedermayr, S. Pimputkar, J. Roberts, R. D. Sanner, T. M. Tillotson, E. van Loef, C. M. Wilson, K. S. Shah, U. N. Roy, R. Hawrami, A. Burger, L. Boatner, W. Choong, and W. W. Moses, “Scintillators with potential to supersede lanthanum bromide,” *IEEE Transactions on Nuclear Science* **56**, 873–880 (2009).
- [4] E. Rowe, P. Bhattacharya, E. Tupitsyn, M. Groza, A. Burger, N. J. Cherepy, S. A. Payne, B. W. Sturm, and C. Pédrini, “A new lanthanide activator for iodide based scintillators: Yb²⁺,” *IEEE Transactions on Nuclear Science* **60**, 1057–1060 (2013).
- [5] P. Beck, N. Cherepy, S. A. Payne, E. L. Swanberg, K. E. Nelson, P. A. Thelin, S. E. Fisher, S. Hunter, B. Wihl, K. S. Shah, R. Hawrami, A. Burger, L. Boatner, M. Momayezi, K. T. Stevens, M. Randles, and D. Solodovnikov, “Strontium iodide instrument development for gamma spectroscopy and radioisotope identification,” *Proceedings of SPIE - The International Society for Optical Engineering* **9213**, 92130N (2014).
- [6] G. Gundiah, G. Bizarri, S. M. Hanrahan, M. J. Weber, E. D. Bourret-Courchesne, and S. E. Derenzo, “Structure and scintillation of Eu²⁺-activated solid solutions in the BaBr₂BaI₂ system,” *Nuclear Inst. and Methods in Physics Research, A* **652**, 234–237 (2011).
- [7] Z. Yan, G. Gundiah, G. A. Bizarri, E. C. Samulon, S. E. Derenzo, and E. D. Bourret-Courchesne, “Eu²⁺-activated BaCl₂, BaBr₂ and BaI₂ scintillators revisited,” *Nuclear Instruments and Methods in Physics Research Section A: Accelerators, Spectrometers, Detectors and Associated Equipment* **735**, 83–87 (2014).
- [8] N. J. Cherepy, G. Hull, A. D. Drobshoff, S. A. Payne, E. van Loef, C. M. Wilson, K. S. Shah, U. N. Roy, A. Burger, L. A. Boatner, W. Choong, and W. W. Moses, “Strontium and barium iodide high light yield scintillators,” *Applied Physics Letters* **92**, 083508 (2008), <https://doi.org/10.1063/1.2885728>.
- [9] E. D. Bourret-Courchesne, G. Bizarri, S. M. Hanrahan, G. Gundiah, Z. Yan, and S. E. Derenzo, “BaBrI:Eu²⁺, a new bright scintillator,” *Nuclear Instruments and Methods in Physics Research Section A: Accelerators, Spectrometers, Detectors and Associated Equipment* **613**, 95–97 (2010).
- [10] G. Bizarri, E. D. Bourret-Courchesne, Z. Yan, and S. E. Derenzo, “Scintillation and optical properties of BaBrI:Eu²⁺ and CsBa₂I₅:Eu²⁺,” *IEEE Transactions on Nuclear Science* **58**, 3403–3410 (2011).
- [11] E. D. Bourret-Courchesne, G. A. Bizarri, R. Borade, G. Gundiah, E. C. Samulon, Z. Yan, and S. E. Derenzo, “Crystal growth and characterization of alkali-earth halide scintillators,” *Journal of Crystal Growth* **352**, 78–83 (2012).
- [12] E. D. Bourret-Courchesne, G. Bizarri, R. Borade, Z. Yan, S. M. Hanrahan, G. Gundiah, A. Chaudhry, A. Canning, and S. E. Derenzo, “Eu²⁺-doped Ba₂CsI₅, a new high-performance scintillator,” *Nuclear Instruments and Methods in Physics Research Section A: Accelerators, Spectrometers, Detectors and Associated Equipment* **612**, 138–142 (2009).
- [13] A. V. Gektin, A. N. Belsky, and A. N. Vasil’ev, “Scintillation efficiency improvement by mixed crystal use,” *IEEE Transactions on Nuclear Science* **61**, 262–270 (2014).
- [14] Z. Yan, T. Shalapska, and E. D. Bourret, “Czochevski growth of the mixed halides BaBrCl and BaBrCl:Eu,” *Journal of Crystal Growth* **435**, 42–45 (2016).
- [15] M. Sonoda, M. Takano, J. Miyahara, and H. Kato, “Computed radiography utilizing scanning laser stimulated luminescence,” *Radiology* **148**, 833 (1983).
- [16] S. Schweizer, “Physics and current understanding of X-Ray storage phosphors,” *Physica Status Solidi Applied Research* **187**, 335–393 (2001).
- [17] S. Schweizer, J. M. Spaeth, and T. J. Bastow, “Generation of F centres and hole centres in the nonstoichiometric x-ray storage phosphor BaFBr,” *Journal of Physics: Condensed Matter* **10**, 9111 (1998).
- [18] E. D. Bourret-Courchesne, G. A. Bizarri, and A. Can-

- ning, “Role of impurities and defects in determining the scintillation properties of mixed halide materials,” (2016), report of Project LB15-V-GammaDetMater-PD3Jf, Advanced Materials for Detectors, unpublished.
- [19] K. Yang, P. R. Menge, J. J. Buzniak, and V. Ouspenski, “Performance improvement of large Sr^{2+} and Ba^{2+} co-doped $\text{LaBr}_3:\text{Ce}^{3+}$ scintillation crystals,” in *2012 IEEE Nuclear Science Symposium and Medical Imaging Conference Record (NSS/MIC)* (IEEE, 2012) pp. 308–311.
- [20] P. Guss, M. E. Foster, B. M. Wong, F. P. Doty, K. Shah, M. R. Squillante, U. Shirwadkar, R. Hawrami, J. Tower, and D. Yuan, “Results for aliovalent doping of CeBr_3 with Ca^{2+} ,” *Journal of Applied Physics* **115**, 34908 (2014).
- [21] F. G. A. Quarati, M. S. Alekhin, K. W. Krämer, and P. Dorenbos, “Co-doping of CeBr_3 scintillator detectors for energy resolution enhancement,” *Nuclear Instruments and Methods in Physics Research Section A: Accelerators, Spectrometers, Detectors and Associated Equipment* **735**, 655–658 (2014).
- [22] N. Shiran, A. Gektin, Y. Boyarintseva, S. Vasyukov, A. Boyarintsev, V. Pedash, S. Tkachenko, O. Zelenskaya, and D. Zosim, “Modification of NaI crystal scintillation properties by Eu-doping,” *Optical Materials* **32**, 1345–1348 (2010).
- [23] K. Yang and P. R. Menge, “Improving γ -ray energy resolution, non-proportionality, and decay time of NaI:Tl^+ with Sr^{2+} and Ca^{2+} co-doping,” *Journal of Applied Physics* **118**, 213106 (2015).
- [24] I. V. Khodyuk, S. A. Messina, T. J. Hayden, E. D. Bourret, and G. A. Bizarri, “Optimization of scintillation performance via a combinatorial multi-element co-doping strategy: Application to NaI:Tl ,” *Journal of Applied Physics* **118**, 84901 (2015).
- [25] T. Shalapska, F. Moretti, E. Bourret, and G. Bizarri, “Effect of Au codoping on the scintillation properties of BaBrCl:Eu single crystals,” *Journal of Luminescence* **202**, 497–501 (2018).
- [26] P. Li, S. Gridin, K. B. Ucer, R. T. Williams, and P. R. Menge, “Picosecond absorption spectroscopy of self-trapped excitons and transient Ce states in LaBr_3 and $\text{LaBr}_3:\text{Ce}$,” *Phys. Rev. B* **97**, 144303 (2018).
- [27] K. B. Ucer, G. Bizarri, A. Burger, A. Gektin, L. Trefilova, and R. T. Williams, “Electron thermalization and trapping rates in pure and doped alkali and alkaline-earth iodide crystals studied by picosecond optical absorption,” *Phys. Rev. B* **89**, 165112 (2014).
- [28] P. Liu, W. L. Smith, H. Lotem, J.H. Bechtel, N. Bloembergen, and R.S. Adhav, “Absolute two-photon absorption coefficients at 355 and 266 nm,” *Phys. Rev. B* **17**, 4620 (1978).
- [29] X. Meng, Y. Wang, H. Jin, and L. Sun, “ BaBrCl:Eu^{2+} : A new promising X-ray storage phosphor,” *J Rare Earths* **24**, 503–505 (2006).
- [30] H. Rabin and C. Klick, “Formation of F centers at low and room temperatures,” *Phys. Rev.* **117**, 1005–1010 (1960).
- [31] R. T. Williams, M. N. Kabler, W. Hayes, and J. P. Stott, “Time-resolved spectroscopy of self-trapped excitons in fluorite crystals,” *Physical Review B* **14**, 725–740 (1976).
- [32] K. S. Song and R. T. Williams, *Self-trapped excitons*, Springer Series in Solid-State Sciences, Vol. 105 (Springer-Verlag, Berlin, Heidelberg, 1993).
- [33] M. J. Marrone, F. W. Patten, and M. N. Kabler, “EPR in triplet states of the self-trapped exciton,” *Physical Review Letters* **31**, 467 (1973).
- [34] A. Wasiela D. Block and Y. Merle d’Aubigne, “ENDOR of the self-trapped exciton in KCl,” *J. Phys. C* **11**, 4201 (1978).
- [35] M.N. Kabler, “Low-temperature recombination luminescence in alkali halide crystals,” *Physical Review* **136**, A1296 (1964).
- [36] R. T. Williams and M. N. Kabler, “Excited-state absorption spectroscopy of self-trapped excitons in alkali halides,” *Physical Review B* **9**, 1897–1907 (1974).
- [37] K. Kan’no, K. Tanaka, and T. Hayashi, “New aspects of intrinsic luminescence in alkali halides,” *Atomic Processes Induced By Electronic Excitation In Non-Metallic Solids*, 253 (1990).
- [38] M. Itoh, S. Hashimoto, and N. Ohno, “Self-trapped exciton luminescence in diluted NaI crystals—relaxation process of excitons in alkali halides—,” *Journal of the Physical Society of Japan* **60**, 4357–4365 (1991).
- [39] G. Kresse and J. Furthmüller, “Efficient iterative schemes for ab initio total-energy calculations using a plane-wave basis set,” *Phys. Rev. B* **54**, 11169 (1996).
- [40] G. Kresse and J. Furthmüller, “Efficiency of ab-initio total energy calculations for metals and semiconductors using a plane-wave basis set,” *Comput. Mater. Sci.* **6**, 15 (1996).
- [41] J. Hutter, M. Iannuzzi, F. Schiffmann, and J. VandeVondele, “cp2k: atomistic simulations of condensed matter systems,” *Wiley Interdisciplinary Reviews: Computational Molecular Science* **4**, 15–25 (2014), <https://onlinelibrary.wiley.com/doi/pdf/10.1002/wcms.1159>.
- [42] M. Guidon, F. Schiffmann, J. Hutter, and J. VandeVondele, “Ab initio molecular dynamics using hybrid density functionals,” *The Journal of Chemical Physics* **128**, 214104 (2008), <https://doi.org/10.1063/1.2931945>.
- [43] D. Dexter, “A theory of sensitized luminescence in solids,” *The Journal of Chemical Physics* **21**, 836–850 (1953).
- [44] N. Itoh and M. Saidoh, “Centres colores et impuretes radiation-induced dynamic motion of interstitial halogen in alkali halides,” in *J. Phys.(Paris) Colloq.*, Vol. 34 (1973) p. C9.
- [45] A. M. T. Allen, J. D. Comins, and P. J. Ford, “Study of defect annealing in γ -irradiated KI by Raman scattering and optical absorption,” *Journal of Physics C: Solid State Physics* **18**, 5783–5792 (1985).
- [46] L. W. Hobbs, A. E. Hughes, D. Pooley, and P. B. Hirsch, “A study of interstitial clusters in irradiated alkali halides using direct electron microscopy,” *Proceedings of the Royal Society of London. A. Mathematical and Physical Sciences* **332**, 167–185 (1973).